Journal of Materials Chemistry A

ROYAL SOCIETY OF CHEMISTRY

PAPER

View Article Online
View Journal | View Issue

Check for updates

Cite this: *J. Mater. Chem. A*, 2025, **13**, 37396

Thermally-driven conformational twist in organic azobenzene linker activates molecular doping effect in thin films of lanthanide MOFs

Umashis Bhoi,[a] Mini Kalyani,[a] Kekkar Subray Ananthram,[b] Sauvik Saha,[a] Aradhana Acharya,[a] Nahid Hassan,[a] Minnu Raj,[a] Kartick Tarafder[b] and Nirmalya Ballav*[a]

Azobenzene-based photo-switchable molecules have shown significant potential in stimuli-responsive systems, especially when incorporated into metal–organic frameworks (MOFs). This study reports thin films of lanthanide-based metal–organic frameworks (Ln-MOFs) with 4,4′-azobenzene dicarboxylic acid (H_2ADA) as the organic linker – Tb-ADA, Eu-ADA, and Gd-ADA – using an electrodeposition method. Upon heating to 400 K, a reversible structural transition was observed *via* variable temperature grazing-incidence X-ray diffraction (GIXRD) and Raman spectroscopy, not due to *trans–cis* isomerization but rather a thermally-induced conformational twist of the ADA linker. Density functional theory (DFT) combined with molecular dynamics (MD) simulations supports this interpretation, revealing high-energy atropisomeric states stabilized by MOF confinement. Molecular doping of these films with 7,7,8,8-tetracyanoquinodimethane (TCNQ) significantly enhanced their electrical conductivity, increasing by two orders of magnitude at 400 K. This enhancement is attributed to improved π–π stacking and charge-transfer interactions facilitated by the conformational twist. Temperature-dependent X-ray photoelectron spectroscopy (XPS) confirmed redox activity in TCNQ@Tb-ADA films, showing reversible conversion between Tb(III) and Tb(IV), with back electron transfer at 400 K restoring Tb(III). These findings introduce a new mechanism of thermally-driven conformational switching in MOFs and open avenues for developing responsive electronic materials based on azobenzene linkers.

Received 16th July 2025
Accepted 27th September 2025

DOI: 10.1039/d5ta05740j

rsc.li/materials-a

Introduction

Photo-switchable molecules are those that can reversibly switch between different isomeric forms in response to light.[1] A well-known example is azobenzene, an archetypal molecular photo-switch, which undergoes *trans*-to-*cis* isomerization when exposed to UV light (typically in the range of 300–400 nm) or when subjected to mechanical stress or electrostatic stimulation. On the other hand, *cis*-to-*trans* isomerization is driven by visible light (wavelengths greater than 400 nm), although this process can also occur thermally in the dark, overcoming a thermal barrier of 1 eV, due to the relative stability of the *trans* isomer.[2–6] This reversible *trans–cis* photo-isomerization of azobenzene typically occurs at room-temperature. The *trans* isomer is planar, while in the *cis* isomer, the benzene rings twist around the C–N bond to minimize steric repulsion, making the *cis* form less stable by 0.6 eV compared to the *trans* form.[5,7] These isomers also differ in the distance between the *para*-C atoms, which decreases from 9 Å in the *trans* isomer to 5.5 Å in the *cis* isomer.[8]

It is well-known that the isomerization of such molecular switches can be controlled or inhibited in a specific solid-state environment. Therefore, the integration of optically switchable azobenzene moieties into metal–organic frameworks (MOFs) has recently attracted significant interest.[9] Depending on the structure of the MOFs, the incorporation of azobenzene may either induce structural distortion through isomerization or have no impact, especially when spatial limitations are present. Within MOFs, the azobenzene moiety can be incorporated in various ways: (i) as an organic linker, (ii) or as a side chain to an organic linker, (iii) or in the void space (pore) *via* synthetic or post-synthetic methods.[10] For example, azobenzene has been incorporated as a guest molecule in a Zn-MOF, where UV light irradiation induced a noticeable structural change from a tetragonal to an *ortho*rhombic phase, due to *trans–cis* isomerization. As a result, the N_2 gas adsorption property was altered, with no uptake observed in the *trans* form and uptake occurring in the *cis* form.[11] In another study, azobenzene was incorporated as an organic linker in a Zn-MOF, which successfully captured CO_2 gas. Interestingly, UV light irradiation led to the release of CO_2 molecules, attributed to *trans–cis*

[a]*Department of Chemistry, Indian Institute of Science Education and Research (IISER), Pune, 411008, India. E-mail: nballav@iiserpune.ac*

[b]*Department of Physics, National Institute of Technology Karnataka (NITK), Surathkal, India*

isomerization.[12] Additionally, when azobenzene was incorporated as part of the side chain of an organic linker in a Zn-MOF, a significant reduction in CO_2 gas uptake was observed after the photochemical treatment.[13] Notably, all of these studies used solvothermal synthesis, and *trans*-to-*cis* isomerization was induced by UV light irradiation on powder samples, with reversibility (*cis*-to-*trans* isomerization) achieved *via* thermal energy or visible light.

The downsizing of MOFs with azobenzene moieties into thin film configurations could further enhance their application potential. For instance, crystalline and uniform thin films of Cu-ADA were fabricated using a layer-by-layer (LbL) method. Infiltration of tetracyanoquinodimethane (TCNQ) molecules enhanced the electrical conductivity of the Cu-ADA thin film, and upon UV-light irradiation, the electrical transport could further be modulated.[14,15] Similarly, atomic/molecular layer deposition (ALD) was employed to fabricate thin films of Fe-ADA MOF, where sequential UV and visible light irradiation induced *trans–cis* isomerization processes, leading to the release and capture of H_2O molecules, respectively.[10]

In this work, we present the fabrication of previously unreported thin films of Lanthanide-ADA MOFs – specifically, Tb-ADA, Eu-ADA, and Gd-ADA – using an electrodeposition technique.[16] Notably, upon heating the films to 400 K and subsequently cooling them back to 300 K, we observed a structural transition indicative of *trans–cis* isomerization of azobenzene. However, on a comprehensive analysis, it was determined that the observed transition was due to the twisting of the benzene rings of the ADA linker. The steric confinement within the MOF stabilizes high-energy P/M isomers of *trans*-azobenzene (so called atropisomers), which are typically transient in free azobenzene molecules. While *trans–cis* isomerization occurs rapidly in free azobenzene moieties under light (on the picosecond scale), this transition becomes significantly slower under confinement.[17] Herein, the thermal excitation within the MOF might drive azobenzene isomerization, but the steric confinement locks the system into a metastable phase. Remarkably, such a conformational twist in the ADA linker activated the molecular doping effect, leading to an increase in the electrical conductance value (close to two orders of magnitude) in the molecularly doped films. This purely thermally-driven, reversible conformational twist represents a novel and unprecedented phenomenon in the field, offering valuable insights into the behavior of azobenzene moieties within confined environments.

Results and discussion

Thin films of Tb-ADA, Eu-ADA, and Gd-ADA MOFs were electrochemically deposited on fluorine-doped tin oxide (FTO) substrates using a three-electrode system, where FTO served as the working electrode, platinum as the counter electrode, and $Ag/AgNO_3$ as the reference electrode (Fig. 1). The deposited films were highly crystalline, as confirmed by out-of-plane grazing-incidence X-ray diffraction (GIXRD) measurements, where all the characteristic peaks aligned with the simulated diffraction pattern of a Tb-ADA MOF synthesized *via*

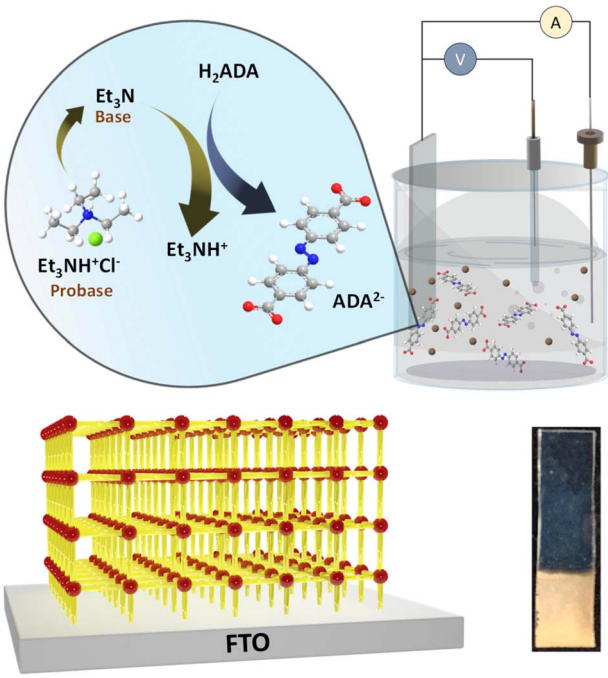

Fig. 1 Schematics of the electrodeposition of Ln-ADA thin films. As an example, optical photograph of the Tb-ADA thin film grown on FTO substrate is shown.

solvothermal methods (CCDC number: 1049582).[18] Pronounced diffraction peaks were observed at 2θ values of ~5.6°, ~11.3°, ~14.3°, ~15.5°, ~16°, ~17.5°, ~21°, and ~23.6° (Fig. S1).

Field-emission scanning electron microscopy (FESEM) images revealed the formation of uniform thin films with an average thickness of approximately 4.5 μm. Elemental mapping through energy-dispersive X-ray spectroscopy (EDXS) confirmed the uniform distribution of all elements within the film (Fig. S2). The chemical bonding between Tb and ADA was examined using FTIR spectroscopy (Fig. S3). Comparison with the spectrum of H_2ADA revealed the disappearance of the peak around 1680 cm^{-1} (corresponding to the free carboxylic –C=O stretch), indicating that the metal–ligand linkage in the Tb-ADA MOF occurs *via* the carboxylate group. This is consistent with the appearance of peaks at approximately 1593 cm^{-1} and 1415 cm^{-1}, as reported in previous studies.[10]

The splitting of the carboxylate stretching peaks suggests a bridging-type coordination.[14] Additionally, the peak at ~1540 cm^{-1} in the Tb-ADA thin film corresponds to the aromatic C–C stretch.[19] To further investigate the chemical bonding, Raman spectroscopy was conducted, revealing vibrational peaks similar to those observed in *trans*-H_2ADA, suggesting the linker is in its *trans* configuration (Fig. S4). Six major peaks were identified in the Tb-ADA MOF at 1143 cm^{-1}, 1191 cm^{-1}, 1406 cm^{-1}, 1458 cm^{-1}, 1503 cm^{-1}, and 1604 cm^{-1}.[7] Peaks at 1143 cm^{-1} and 1191 cm^{-1} are attributed to –C–N= stretching modes, while the modes at 1406 cm^{-1}, 1458 cm^{-1} (which was at 1466 cm^{-1} in free *trans*-H_2ADA molecule) and 1503 cm^{-1} corresponds to in-plane ring bending with slight coupling to the –N=N– stretch. The peak at 1604 cm^{-1}

corresponds to C–C stretch/bend,[20] which appears broad for the free *trans*-H_2ADA molecule, whereas it becomes sharp in the MOF.

Variable temperature GIXRD measurements from 300 K to 420 K were performed to evaluate the thermal and phase stability of the Tb-ADA thin films (Fig. 2a, b and S5). Unlike the temperature-dependent XRD patterns of an earlier reported Gd-ADA MOF,[21] which remained nearly unchanged, a distinct shift in peak positions was observed at 400 K for the Tb-ADA MOF, particularly in the higher 2θ range, suggesting a structural change. This change persisted up to 420 K and fully reverted upon cooling back to 300 K, indicating thermal reversibility. Additionally, the decrement in intensity and peak broadening at 2θ range of ~14–16° during heating suggests a reduction in crystallinity, likely due to the structural change. A similar phenomenon was observed in thin films of Fe-ADA MOF, where reversible photo-isomerization of azobenzene from *trans* to *cis* was reported by monitoring the GIXRD patterns.[10] Our observations also align with this behavior, apparently suggesting a thermal-driven reversible *trans–cis* isomerization, however, it has not been previously reported for this system, thereby necessitating a rather critical investigation.

To probe this structural change in detail and to test the hypothesis of *trans–cis* isomerization as its origin, we employed temperature-dependent Raman spectroscopy (Fig. 2c). Simulated Raman spectra for the *trans* and *cis* isomers of H_2ADA revealed sufficiently distinct vibrational signatures, enabling differentiation between the two isomers (Fig. 2d). The experimentally recorded Raman spectra at room-temperature (~300 K) and at ~400 K displayed similar peak positions but with a significant decrease in the intensity of vibrational modes in the 1400–1600 cm^{-1} region at 400 K, clearly ruling out the possibility of *trans–cis* isomerization within this temperature range. Instead, the thermal energy gained facilitated the system to undergo a conformational change that could supposedly lead to a *trans–cis* isomerization, however, got restricted due to steric constraints. Therefore, the reduction in intensity can be attributed to the loss of conjugation due to the twisting of the benzene rings of the ADA linker, which lowers the polarizability consequently reduces the Raman intensity.[20] This interpretation is corroborated by the theoretical insights gained from the density functional (DFT) calculations combined with molecular dynamic (MD) simulations performed on the Tb-ADA system. Energy optimized structures at 300 K and 400 K exhibited significantly twisted conformations of the ADA linker featuring respective dihedral angle (Φ_D) of 26° and 64°, representing high-energy conformations when compared to *trans* and *cis* isomers (Fig. 3). Notably, azobenzene derivatives are well-known for their orientational disorder wherein they adopt one of their two possible conformations that are related by rotation along the long axis of the molecule – so called 'pedal-like' motion.[22–24] This combined experimental and computational evidences therefore support a thermally-driven conformational twisting of

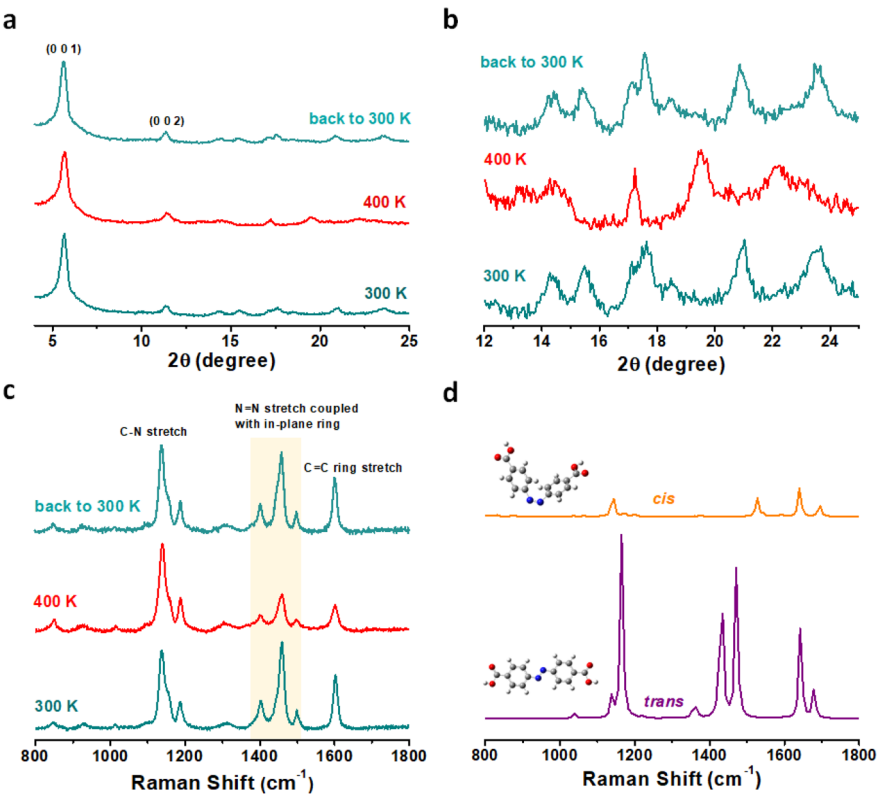

Fig. 2 Variable-temperature (a) GIXRD pattern, (b) zoomed-in GIXRD pattern, (c) Raman spectra recorded on Tb-ADA thin film; and (d) simulated Raman spectra of ADA (*cis* and *trans*) from theoretical calculations.

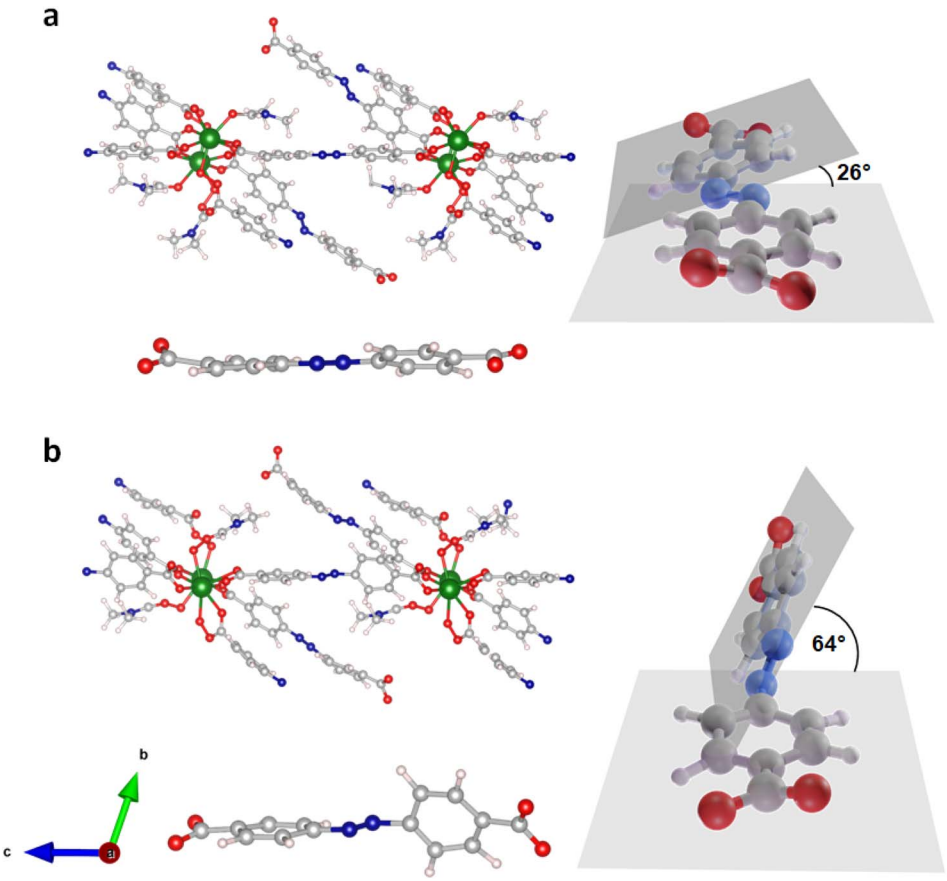

Fig. 3 Energy-optimized structural insights for the Tb-ADA system at (a) 300 K, and (b) 400 K obtained from combined DFT-MD investigations.

the benzene rings in the ADA linker rather than a definitive *trans–cis* isomerization.

Thin films of Eu-ADA and Gd-ADA MOFs, which are isostructural to Tb-ADA, were also fabricated and characterized (Fig. S6 and S9). Temperature-dependent studies revealed similar behavior to Tb-ADA, where an increase in temperature resulted in reduced GIXRD peak intensities, peak broadening, and the appearance of new diffraction peaks due to structural changes in the Eu-ADA MOF (Fig. S7). Temperature-dependent Raman spectra of Eu-ADA and Gd-ADA also exhibited a decrease in intensity, particularly in the 1400–1600 cm^{-1} range, mirroring the behavior observed in Tb-ADA, supporting the thermal-driven structural change in these MOFs and the conformational twist in the azobenzene linker (Fig. S8 and S10). To confirm that the observed conformational change occurred specifically in the ADA linker within the MOF and not in free H_2ADA molecules, temperature-dependent studies were conducted on free H_2ADA. Variable temperature GIXRD patterns showed no shift in peak positions at 300 K and 400 K (Fig. S11), and Raman spectra recorded at 400 K did not differ significantly from those obtained at 300 K (Fig. S12). These results indicate that free H_2ADA does not undergo any conformational change.

Transition metal ions typically exhibit coordination numbers of four, five, or six, while lanthanide ions generally show coordination numbers greater than eight, offering more flexibility in the metal–ligand coordination sphere. The smaller coordination spheres of transition metals, such as Cu, may cause steric hindrance, limiting or preventing any conformational change. To explore whether the metal center influences thermally-driven conformational change, similar temperature-dependent studies were conducted on Cu-ADA thin films. The GIXRD patterns and Raman spectra of Cu-ADA films showed no changes upon heating, in contrast to the behavior observed in Ln-ADA MOFs, highlighting the unique thermally-driven structural change in Ln-based MOFs (Fig. S13 and S14).

MOFs are known to be intrinsically poor conductors of electricity due to the limited overlap between the π-orbitals of the organic ligands and the d-orbitals of the metal ions.[25] Temperature-dependent current–voltage (*I–V*) profiles were measured on thin films of Tb-ADA and Gd-ADA, at both room-temperature (300 K) and at 400 K (Fig. S15a and S15b) which suggested that the electrical conductance value remained almost unchanged with increasing the temperature *viz.* electrically insulating in nature. A promising strategy to enhance the electrical conductivity of MOFs involves infiltrating the framework pores with redox-active molecules like TCNQ (7,7,8,8-tetracyanoquinodimethane) – a molecular doping strategy.[26–28] Accordingly, Tb-ADA and Gd-ADA thin films were doped with TCNQ following a reported protocol and molecularly doped thin films of TCNQ@Tb-ADA and TCNQ@Gd-ADA

were fabricated.[15] To confirm the presence of TCNQ in the thin films, Raman spectroscopy measurements were performed, and the signature peak at 1206 cm^{-1} corresponding to the C═C–H bending vibration was identified (Fig. S16). GIXRD patterns on TCNQ@Tb-ADA and TCNQ@Gd-ADA thin films revealed no additional peak and therefore, structural integrity was retained upon molecular doping (Fig. S17 and S18).

To investigate the effect of TCNQ doping on the electrical transport properties, temperature-dependent *I–V* profiles were recorded on TCNQ@Tb-ADA and TCNQ@Gd-ADA thin films, and the values demonstrate that the MOF thin films are less conductive (Table S1). Upon increasing the temperature, a dramatic increase in current value (close to two orders of magnitude), in comparison to the value at 300 K, was observed at 400 K for TCNQ@Tb-ADA thin film (Fig. 4a (sample 1) and S19). A similar effect was also noted for TCNQ@Gd-ADA thin film (Fig. S20). Specifically, for TCNQ@Tb-ADA thin film, conductance values of $\sim 1.0 \times 10^{-12}$ S and $\sim 5.0 \times 10^{-10}$ S at ~300 K and 400 K were realized. Interestingly, in the temperature range 300 K to 360 K (Fig. 4b and S21), no appreciable increase in the electrical conductance value was noted and such a sudden increment at 400 K is likely attributed to a thermally-induced conformational change (twisting) of the benzene rings of the ADA linker, which may facilitate improved π–π stacking interactions with the doped TCNQ, thereby creating a more efficient charge-transfer pathway and ultimately improving the electrical conductivity (Table S2). *I–V* measurements on multiple samples have been explored to check the reproducibility of the samples, and the average conductance value at 400 K for TCNQ@Tb-ADA thin films was found to be $\sim 2.0 \times 10^{-10}$ S (Fig. S22). Additionally, TCNQ@Tb-ADA thin films exhibited long-term cycling stability of the conductance over multiple heating–cooling cycles, showing potential use in electronic applications (Fig. S23). In the temperature-dependent Raman spectra, a blue-shift from 1386 cm^{-1} (300 K) to 1389 cm^{-1} (400 K) could be an indication of enhanced coordination of TCNQ with the Ln ion (Fig. S24). A better understanding of the temperature-dependent charge-transfer within TCNQ@Tb-ADA thin film, X-ray photoelectron spectroscopy (XPS) was employed. For pristine Tb-ADA thin film, the photoemission signal of Tb $3d_{5/2}$ exhibited a characteristic peak at ~1239.1 eV, accompanied by its associated satellite features, indicating almost exclusively the presence of Tb(III) at both 300 K and 400 K (Fig. S25). In contrast, XPS spectrum recorded on TCNQ@Tb-ADA thin film at 300 K revealed the presence of Tb(III) (binding energy value of Tb $3d_{5/2}$ at 1239.1 eV) and a higher binding energy peak at 1244.3 eV which can be assigned to be due to Tb(IV) (Tb $3d_{5/2}$), each Tb(III) and Tb(IV) with their respective satellite features. This observation highlights the strong electron-accepting nature of TCNQ, which facilitates partial oxidation of Tb(III) to Tb(IV),thereby generating mixed-valence Tb(III)–Tb(IV) redox centres within the system. Interestingly, at 400 K, almost exclusively suggests that the thermally-induced conformational twist in the ADA linker activates back electron transfer to stabilize the Tb(III) oxidation state.

This redox behaviour involving f-electrons is in strong contrast with the observations involving d-electrons, where pristine Cu-ADA film exhibited presence of almost exclusive Cu(II) species, while post-infiltration XPS data revealed additional Cu(I) signals in TCNQ@Cu-ADA thin film, indicative of Cu(II)–Cu(I) redox centres in the system.[15] The distinct redox profiles in the Tb-ADA and Cu-MOF systems also emphasize the importance of metal-specific charge-transfer in the molecular doping phenomenon. Likewise, Tb 3d XPS spectra, N 1s XPS spectral features of TCNQ@Tb-ADA at 300 K and 400 K were distinctively different (Fig. 5a and b). At 300 K, the respective photoemission signals at binding energy of ~400.2 eV and ~394.8 eV are assigned to be due to –N═N– in ADA denoted as N(ADA) and Tb 4s; while the peaks at ~398.0 eV and ~396.5 eV are assigned to be due to the presence of TCNQ (marked as N(TCNQ)) in monoanion and dianion forms in the system – so that TCNQ dianion is charged balanced with Tb(IV). Remarkably, at 400 K, almost exclusive presence of TCNQ monoanion was realized and therefore endorsing the electron transfer from TCNQ dianion to Tb(IV) finally leading to a charge balance system with Tb(III).[16] Additionally, TCNQ@Cu-ADA displayed more continuous temperature dependent *I–V* profiles, typically a thermally-activated charge transport as in semiconductors.[15]

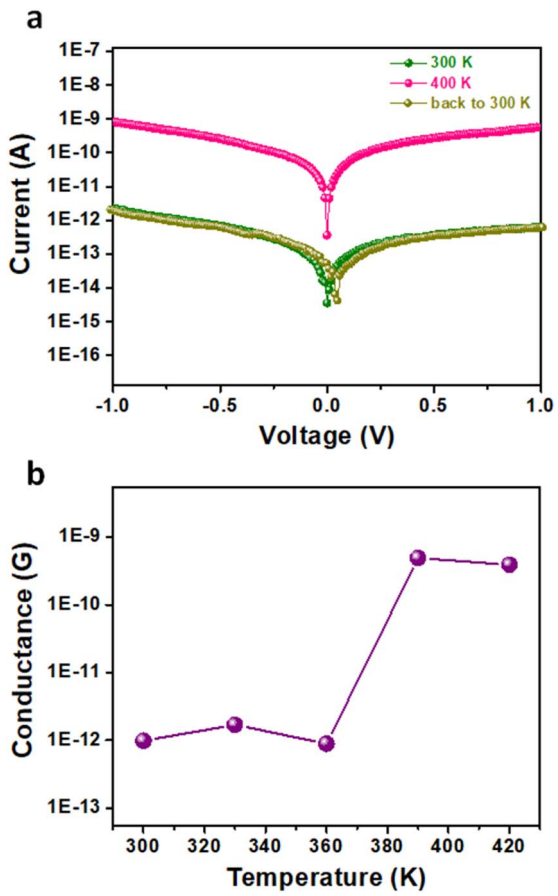

Fig. 4 Variable-temperature (a) current (*I*) *vs.* voltage (*V*) profiles; and (b) extracted conductance (G) *vs.* temperature plot for TCNQ@Tb-ADA thin film.

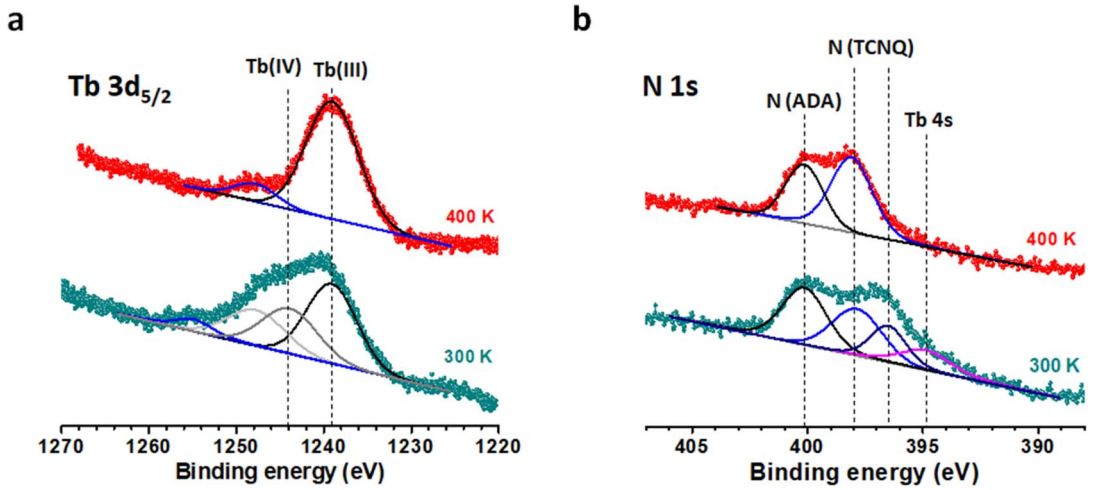

Fig. 5 Variable-temperature XPS spectra of TCNQ@Tb-ADA thin film showing the (a) Tb $3d_{5/2}$, and (b) N 1s photoemission signals.

Conclusions

In conclusion, this study reports the successful fabrication and characterization of thin films of Tb-ADA, Eu-ADA, and Gd-ADA *via* electrodeposition technique, revealing a unique thermally-driven conformational twist of the azobenzene-based ADA linker at an elevated temperature. Contrary to classical *trans–cis* photo-isomerization, this conformational twist is sterically confined within the MOF framework, leading to a metastable, high-energy atropisomeric state. Remarkably, such a conformational twist significantly enhances electrical conductance – by two orders of magnitude – when molecularly doped with TCNQ. The observed increase in conductance is attributed to improved π–π stacking and a thermally-activated charge-transfer pathway. Moreover, temperature-dependent XPS studies confirmed redox transitions between Tb(III)–Tb(IV), highlighting the much contrastive role of f-electrons with respect to d-electrons, in modulating the electrical transport property. Our work not only advances understanding of azobenzene behavior in confined environments but also opens pathways for designing responsive MOF-based materials with intricate complexity, offering promising implications for electronic device applications.

Conflicts of interest

There are no conflicts to declare.

Data availability

All data supporting the findings of this study are available within this article and its SI. Supplementary information is available. See DOI: **https://doi.org/10.1039/d5ta05740j**.

Acknowledgements

Financial support from IISER Pune, India is gratefully acknowledged. U. B. thanks UGC (India) for the Research Fellowship. K. T. acknowledges C-DAC for providing the computational facility in PARAM Utkarsh. The support and the resources provided by "PARAM Brahma Facility" under the National Supercomputing Mission, Govt. of India at IISER Pune are gratefully acknowledged.

Notes and references

1 M.-M. Russew and S. Hecht, *Adv. Mater.*, 2010, **22**, 3348–3360.
2 G. S. Hartley, *Nature*, 1937, **140**, 281.
3 N. Campbell, A. W. Henderson and D. Taylor, *J. Chem. Soc., Chem.*, 1953, 1281–1285, DOI: **10.1039/JR9530001281**.
4 H. M. D. Bandara and S. C. Burdette, *Chem. Soc. Rev.*, 2012, **41**, 1809–1825.
5 I. Conti, M. Garavelli and G. Orlandi, *J. Am. Chem. Soc.*, 2008, **130**, 5216–5230.
6 I. C. D. Merritt, D. Jacquemin and M. Vacher, *Phys. Chem. Chem. Phys.*, 2021, **23**, 19155–19165.
7 C. R. Crecca and A. E. Roitberg, *J. Phys. Chem. A*, 2006, **110**, 8188–8203.
8 B. Zhang, Y. Feng and W. Feng, *Nanomicro Lett.*, 2022, **14**, 138.
9 C. L. Jones, A. J. Tansell and T. L. Easun, *J. Mater. Chem. A*, 2016, **4**, 6714–6723.
10 A. Khayyami, A. Philip and M. Karppinen, *Angew. Chem., Int. Ed.*, 2019, **58**, 13400–13404.
11 N. Yanai, T. Uemura, M. Inoue, R. Matsuda, T. Fukushima, M. Tsujimoto, S. Isoda and S. Kitagawa, *J. Am. Chem. Soc.*, 2012, **134**, 4501–4504.
12 R. Lyndon, K. Konstas, B. P. Ladewig, P. D. Southon, P. C. J. Kepert and M. R. Hill, *Angew. Chem., Int. Ed.*, 2013, **52**, 3695–3698.
13 J. Park, D. Yuan, K. T. Pham, J.-R. Li, A. Yakovenko and H.-C. Zhou, *J. Am. Chem. Soc.*, 2012, **134**, 99–102.
14 J.-L. Zhuang, K. Lommel, D. Ceglarek, I. Andrusenko, U. Kolb, S. Maracke, U. Sazama, M. Fröba and A. Terfort, *Chem. Mater.*, 2011, **23**, 5366–5374.

15 S. Saha, T. M. Jose, M. Kalyani, N. Hassan, U. Bhoi, A. Ugale and N. Ballav, *J. Chem. Sci.*, 2025, **137**, 26.
16 U. Bhoi, S. Ray, S. Bhand, P. Ninawe, D. Roy, S. Rana, K. Tarafder and N. Ballav, *ACS Energy Lett.*, 2023, **8**, 4465–4473.
17 L. Pesce, C. Perego, A. B. Grommet, R. Klajn and G. M. Pavan, *J. Am. Chem. Soc.*, 2020, **142**, 9792–9802.
18 B. Fernández, I. Oyarzabal, J. M. Seco, E. S. Sebastián, D. Fairen-Jiménez, S. Gómez-Ruiz, A. Salinas-Castillo, A. J. Calahorro and A. Rodríguez-Diéguez, *Polymers*, 2016, **8**, 39.
19 T. Sato, Y. Ozaki and K. Iriyama, *Langmuir*, 1994, **10**, 2363–2369.
20 Y. B. Zheng, J. L. Payton, C.-H. Chung, R. Liu, S. Cheunkar, B. K. Pathem, Y. Yang, L. Jensen and P. S. Weiss, *Nano Lett.*, 2011, **11**, 3447–3452.
21 S. Zhang, E. Duan, Z. Han, L. Li and P. Cheng, *Inorg. Chem.*, 2015, **54**, 6498–6503.
22 J. Harada and K. Ogawa, *J. Am. Chem. Soc.*, 2001, **123**, 10884–10888.
23 J. Harada and K. Ogawa, *Chem. Soc. Rev.*, 2009, **38**, 2244–2252.
24 A. Mohan, D. Sasikumar, V. Bhat and M. Hariharan, *Angew. Chem., Int. Ed.*, 2020, **59**, 3201–3208.
25 L. S. Xie, G. Skorupskii and M. Dincă, *Chem. Rev.*, 2020, **120**, 8536–8580.
26 A. Prasoon, B. Dhara, D. Roy, S. Rana, S. Bhand and N. Ballav, *Chem. Sci.*, 2019, **10**, 10040–10047.
27 P. Sindhu and N. Ballav, *Inorg. Chem.*, 2023, **62**, 10887–10891.
28 A. A. Talin, A. Centrone, A. C. Ford, M. E. Foster, V. Stavila, P. Haney, R. A. Kinney, V. Szalai, F. El Gabaly, H. P. Yoon, F. Léonard and M. D. Allendorf, *Science*, 2014, **343**, 66–69.